International Journal of Precision Engineering and Manufacturing
https://doi.org/10.1007/s12541-025-01338-y

Online ISSN 2005-4602
Print ISSN 2234-7593

REGULAR PAPER

Improving the Prediction Accuracy of Surface Roughness in the Boring Process using Integrated Machine Learning Methods

Aslan Akdulum[1] · **Yunus Kayir**[2]

Received: 31 May 2025 / Revised: 7 August 2025 / Accepted: 12 August 2025
© The Author(s), under exclusive licence to Korean Society for Precision Engineering 2025

Abstract
Precision boring is essential for achieving high-quality holes, yet attaining the desired surface roughness remains a challenge due to the confined machining environment and the instability of long, slender boring bars. Although simple analytical models exist, they often fall short in accurately predicting surface roughness in boring operations. In machining applications, conducting extensive experiments is limited by high costs and time constraints; thus, small sampling problems occur in the prediction models. Therefore, it is necessary to establish high-accuracy surface roughness prediction models with optimized input features. In this study, an integrated machine learning-based methodology is proposed to overcome these challenges. The approach includes ranking input features by importance, incorporating physics-based features, expanding the feature space, and generating virtual samples to enrich the training data. The results indicate that the proposed model improves prediction accuracy by 27%. The most significant enhancement was observed when virtual samples were added after expanding the feature set with physics-based parameters. These findings contribute to more precise and cost-effective planning in boring operations.

Keywords Machine learning · Boring process · Surface roughness prediction · Feature augmentation · Virtual sampling · Physics-based features

1 Introduction

In industries where high-precision, quality holes are desired, the boring operation plays a crucial role as the final process [1]. Boring is a process performed to enlarge previously created holes, such as drilling, forged, punched, or cored, and bring them to a final size and quality [2]. Especially in industries such as mold making and automotive, the boring process is very important in terms of product cycle time [3]. In the boring process, the constraints on hole diameter and depth result in boring bars having a long and slender structure [4]. Due to this geometry, process stability becomes highly dependent on the proper selection of boring parameters. In this context, the boring parameters evaluated in the present study include feed rate, insert radius, radial depth of cut, coating type, roughness measuring distance, and cutting speed. To provide a clearer understanding of the boring process and the associated parameters, a schematic representation of the boring operation is presented in Fig. 1. This situation requires optimum determination of boring parameters according to workpiece material, boring bar, and cutting insert [5]. Improperly selected boring parameters can lead to increased cutting forces [6], vibrations, uncontrollable centrifugal forces, and various dynamic instabilities [7, 8]. These issues negatively impact hole quality and, consequently, surface roughness (Ra) [9]. Poor hole quality often necessitates secondary operations, resulting in time delays and financial losses [10].

In order not to negatively affect the machining process and to make efficient process planning, the surface roughness must be modeled and estimated with high accuracy according to the input properties determined before the cycle. Thus, the quality control process can become more efficient by eliminating the need for secondary operations after the

✉ Aslan Akdulum
aslanakdulum@hacettepe.edu.tr

✉ Yunus Kayir
ykayir@gazi.edu.tr

[1] Department of Machinery and Metal Technologies, Başkent OSB Vocational School of Technical Sciences, Hacettepe University, Ankara, Türkiye, Turkey

[2] Department of Manufacturing Engineering, Faculty of Technology, Gazi University, Ankara, Turkey

Published online: 23 September 2025

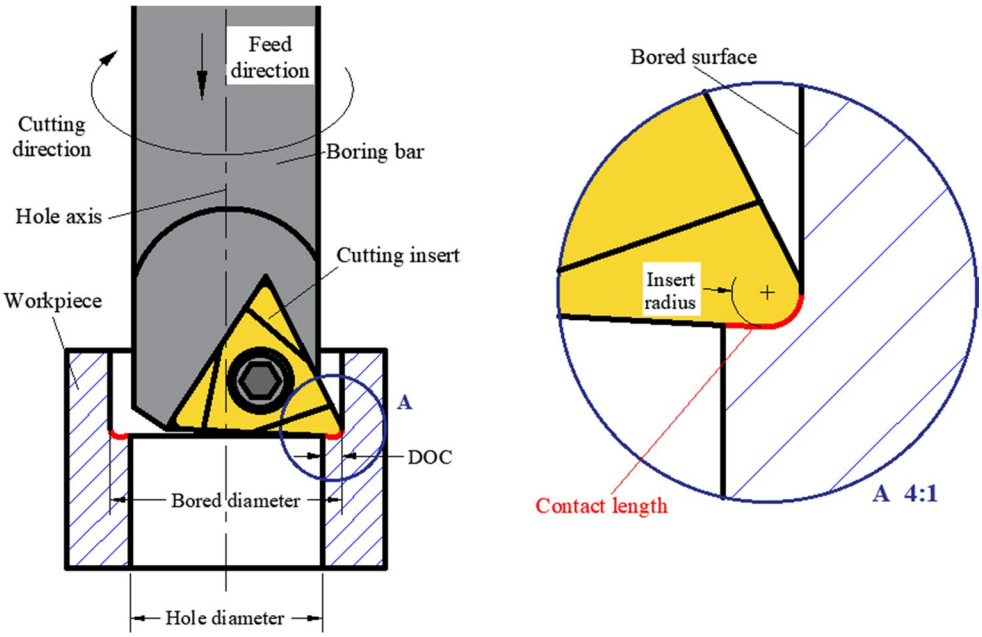


Fig. 1 Boring process diagram

machining process [11]. Additionally, cycle time and costs can be reduced by optimizing processing parameters [12]. Continuity in final product quality can be achieved as a result of proactive measures such as early detection and correction of possible production errors. However, there are not enough studies for modeling and estimating boring surface roughness in milling machines. When the available research is analyzed, the influences of boring variables on boring surface roughness are often investigated. For example, the influences of different cutting insert geometry and different cubic boron nitride (CBN) ratios on surface roughness [13], the influences of low-frequency vibration [14], the impacts of nose radius and coolant [15], the effects of depth of cut [16], and the effects of spindle speed and feed [1] were investigated. Surface roughness was simulated in two and three dimensions to take into account the kinematic motion deviations between the workpiece and the cutting tool [17]. Surface roughness was calculated using a regression equation that took into account the depth of cut, spindle speed, tool radius, and feed rate [18]. A mathematical model was developed with the help of variance analysis [19]. However, the established models and calculated equations are quite insufficient and need to be supported by new studies. In addition, more comprehensive research is required that includes the cutting nose radius and cutting coating type, which have a significant effect on hole quality. Instead of existing simple empirical relationships, more advanced data-based methods are needed. Thus, the relationship network between boring parameters and boring surface roughness can be determined more clearly, and boring quality can be increased. Therefore, there is a need for models that can effectively model the boring surface roughness and predict it with high accuracy.

In order to establish more effective prediction models, studies are intensifying on artificial intelligence-supported machine learning (ML) methods, which are becoming increasingly popular. With ML methods, more flexible models can be established compared to traditional statistical methods, thus stronger prediction performance can be achieved [20]. In addition to being used in different fields, they are also used to establish models in machining processes [21]. For example, there are studies in the topics of drilling [22], milling [23, 24], turning [11, 25, 26], selective laser melting [27], and electrical discharge machining [28]. As a result, the ML method can effectively model the surface roughness obtained during the boring process.

It is not possible to conduct many experiments in the machining test process due to constraints such as material, cost, and time [12]. Therefore, low-dimensional training sets are used to build prediction models, and model performance is negatively affected [29]. In addition, this situation causes small sample size problems such as unbalanced distribution and poor representation of the collected samples [30]. To overcome these problems, methods such as ranking the features according to their importance [25, 31], adding physics-based features [32, 33], increasing the feature size [27, 34], and creating virtual samples [12, 35] are used. Examining these methods in detail and comparing them with each other is very important, especially for areas with small sample datasets, such as machining processes. In-depth comparison of the modeling and estimation performance of the methods and investigation of whether their successive use will create a synergistic effect seems to be very important in solving small sample problems. There is the potential to build higher-performing models

by integrating various ML methods. Therefore, innovative methods need to be researched or developed to increase the predictive success of models with small-sized training sets.

The current study aims to accurately measure the surface roughness caused by the precision boring operation of a 1.2738 workpiece on a milling machine. For this purpose, methods such as using the boring parameters as input parameters, ranking the features according to their importance, adding physics-based features, increasing the features with feature engineering, and adding virtual data points to the training set were used. In addition, unlike traditional methods such as Anova and Pearson correlation used to determine the importance levels of features, the use of Shapley Additive Explanations (SHAP) values has been suggested. The proposed methods were used separately and successively to determine the method that can provide the most effective solution to small sampling problems. The prediction performances of the established models were carefully examined in depth and compared. Thus, it is aimed at increasing the prediction performance for datasets with small data sizes. The proposed integrated strategy has the ability to considerably enhance prediction performance on datasets with small sample numbers.

The study's distinguishing contributions are listed below.

- The surface roughness obtained during the precision boring process on the milling machine was modeled and compared using several ML approaches.
- Input parameters were ranked according to SHAP value, and individual effects of features on output response were examined.
- The effects of physics-based features added to the boring parameters on the prediction performance were investigated.
- The effect of increasing the size of features with feature engineering on performance success was investigated.
- The integrated performance of all methods was meticulously studied in depth.
- The effects of virtual samples added to the training set on the prediction performance were compared.

The remainder of the work is reviewed under the subsequent headings: Section 2 outlines how experiments are carried out, including measurement, data collection, dataset preparation, and model and performance metric setup. Section 3 and Section 4 summarizes the study's findings and compares the proposed approaches to one another and to the literature in detail. Section 5 highlights the study's primary findings and addresses the identified implications. It also makes suggestions for promising future studies.

2 Materials and Methods

2.1 Conducting Experiments, Taking Measurements, and Collecting Data

To model and determine the link between boring characteristics and surface roughness, precision boring experiments were tested on the machine tool shown in Fig. 2. The experimental setup used in this study has been previously validated and successfully applied in different investigations to estimate feed force and analyze the effects of machining parameters on cutting torque [6, 36, 37]. Therefore, its reliability and suitability for similar machining studies have been demonstrated in the literature. The hole's surface roughness was then measured with the apparatus illustrated in the figure. The experimental setup

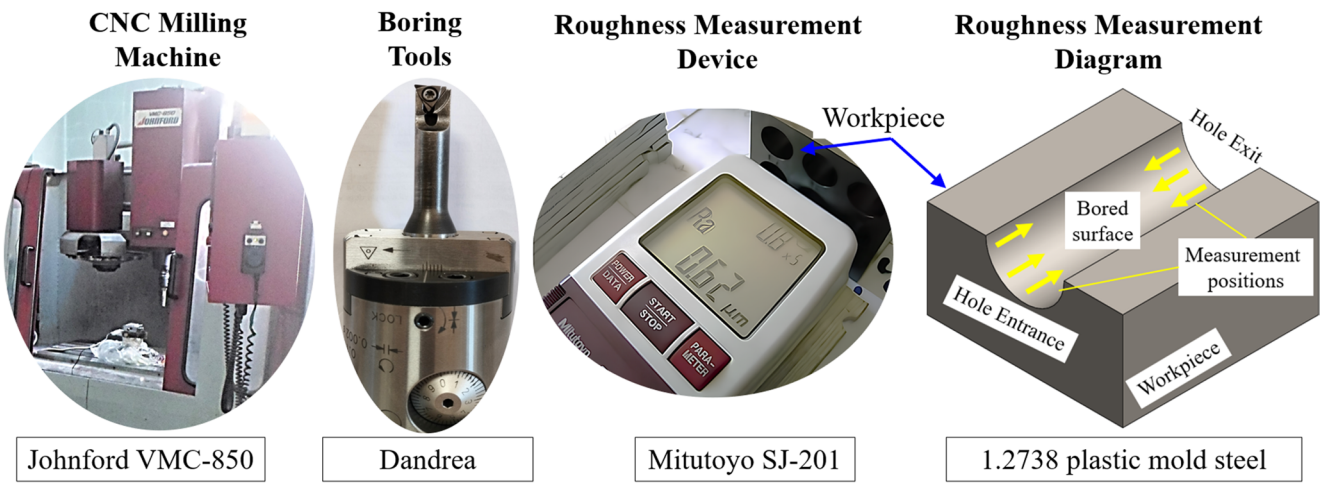


Fig. 2 Experimental setup of boring process and surface roughness measurement

Table 1 Chemical components of 1.2738 plastic mold steel

	Mo	Cr	Si	Mn	C	Ni	Fe
1.2738	0.2	1.9	0.3	1.5	0.4	1	Balance

Table 2 The determined mechanical characteristics of 1.2738 plastic mold steel

	Elongation (%)	Hardness, Rockwell C (HRC)	Tensile strength (Mpa)	Yield strength (Mpa)
1.2738	8.15	35.5	975	807

Table 3 Input features and levels

Input features	Levels		
FR, mm/rev	0.04	0.06	0.09
DOC, mm	0.2	0.3	0.5
CS, mm/min	130	162	203
IR, mm	0.2	0.4	
CT	1-Uncoated	2-Coated	
MD, mm	5	30	

was intended to accurately predict surface roughness during the precision drilling of 1.2738 plastic mold steel.

Prismatic 1.2738 material with a thickness of 35 mm was used in the experimental research. This material is especially preferred in the mold-making industry in the process of obtaining die and mould cavities [38]. In the experimental setup, the workpiece is fixed, and the boring operation is performed by both rotation and feed of the cutting tool. The chemical components of the workpiece material used are exhibited in Table 1, while the mechanical properties acquired as a result of the tensile test and hardness measurement are exhibited in Table 2. The table's values represent the averages of three tests.

Prior to boring, the holes were drilled by ordinary helical drills of varied sizes to reach the correct measure. Then, precise hole enlargement was carried out throughout. The brand of the tools and cutting inserts used for boring was Dandrea. Experiments were carried out with Taguchi L36 ($2^2 \times 3^3$) experimental design. Roughness measurements were taken from the entrance and exit of the hole for 36 parts. Therefore, a dataset with 72 data points was obtained. The number of input features determined in the boring process is six. These are feed rate (FR), insert radius (IR), radial depth of cut (DOC), coating type (CT), roughness measuring distance (MD), and cutting speed (CS), as shown in Table 3. The roughness measuring distance (MD) was considered as an input parameter, as variations in surface roughness measurements can be influenced by factors such as tool wear, cutting forces, and local surface defects, which become more representative over longer evaluation lengths. Boring settings were obtained by reviewing cutting tool handbook suggestions and research.

Table 4 Characteristics of cutting inserts

Material	Coating	Radius	Insert geometry
Cermet	No	0.2 mm	TPGX090202L DC100
Cermet	No	0.4 mm	TPGX090204L DC100
Cermet	Yes	0.2 mm	TPGX090202L DC100T
Cermet	Yes	0.4 mm	TPGX090204L DC100T

As the boring bar attached to the bus head moves along the hole axis, different mechanical and dynamic effects occur. These varied impacts have a direct impact on hole quality. One of the most crucial signs of hole functionality is the surface roughness within the hole. The surface roughness inside the hole measurements were made for all drilled workpieces. For the measurements, a "Mitutoyo SJ-201" model roughness measuring device was used. The measurement method in the device was the follower tip method; scanning length was 5 mm, cut-off was 0.8 mm, and scanning speed was 0.5 mm/s. Then, the entrance and exit of the hole were measured three times with the surface roughness device. The final measurement value was calculated via the mean of the measurements collected.

In order to attain the final hole diameter of 14 mm, appropriate boring tools were employed, achieving a dimensional accuracy of 1 micron in radius. Prior to the boring process, pilot holes were pre-drilled using drill bits with diameters carefully selected based on the specified depths of cut (DOC) values of 0.2 mm, 0.3 mm, and 0.5 mm. These pilot hole diameters—measuring 13 mm, 13.4 mm, and 13.6 mm, respectively—were deliberately smaller than the target final diameter. Detailed geometric characteristics and specifications of the cutting inserts utilized in the process are provided in Table 4.

3 Proposed Boring Surface Roughness Prediction Methods

This study is aimed at estimating the internal hole roughness resulting from the precision boring process of a 1.2738 plastic mold steel workpiece with high accuracy. AdaBoost (AB), XGBoost (XGB), Gradient Boosting (GB), and Bagging Regressor (BR) ML algorithms were determined for the prediction of the boring surface roughness by precise modeling. The selected algorithms were preferred due to their high prediction accuracy on datasets with small sample sizes and their robustness against noisy data. These algorithms are powerful in modeling complex relational structures and are particularly effective in regression problems. For instance,

XGB is an advanced boosting algorithm that optimizes tree-based learning structures and includes strong mechanisms to prevent overfitting [39]. GB improves prediction accuracy by iteratively reducing model error through successive learning [40]. AB combines weak learners to form a strong predictor and stands out especially due to its model diversity [41]. BR, on the other hand, enhances model generalization by reducing variance through sampling and model diversity [42].

The hyperparameters used in these algorithms were determined based on both literature recommendations and empirical experimentation. For each algorithm, hyperparameter optimization of key parameters (such as learning rate, number of trees, maximum depth, and subsampling rate) was performed using the grid search method. Although computationally intensive, this approach systematically explores a predefined parameter space, improving model accuracy while helping to avoid overfitting.

A cross-validation (5-fold) procedure was employed to prevent set overfitting and produce more generalizable results. A baseline dataset consisting of 72 data points, including six input features and one output response, was obtained. 50 of these data were employed in the training set and 22 in the test set. Data processing, dataset preparation, virtual sample generation, model establishment, and verification processes were performed with the phyton programming language.

3.1 Preparation of Datasets

Various dataset groups have been prepared for effective modeling of the surface roughness achieved as a result of the boring operation and its quantitative estimation with high accuracy. The goal of preparing these diverse groups is to thoroughly compare the results of various ML approaches for estimating boring surface roughness. These groups have been prepared for the plan of comparing different ML methods, such as direct use of boring parameters, ranking features according to their importance, adding physics-based features, increasing feature dimensionality with feature engineering, and generating virtual sampling. The schema of the prepared groups and datasets is given in Fig. 3. As a result of the operations, a total of 188 regression models were established and examined. These added features include penetration rate (denoted as Vf), material removal rate (MRR), cutting duration (CD), chip area (CA), chip perimeter (CP), and cutting contact length (CL). The primary dataset, referred to as PD (short for Principal Dataset), was created. In this study, six boring parameters and six physics-based features were combined to form a total of twelve features. This newly formed group was labeled as SD, representing the Secondary Dataset. Furthermore, the expanded version of the PD dataset was designated as

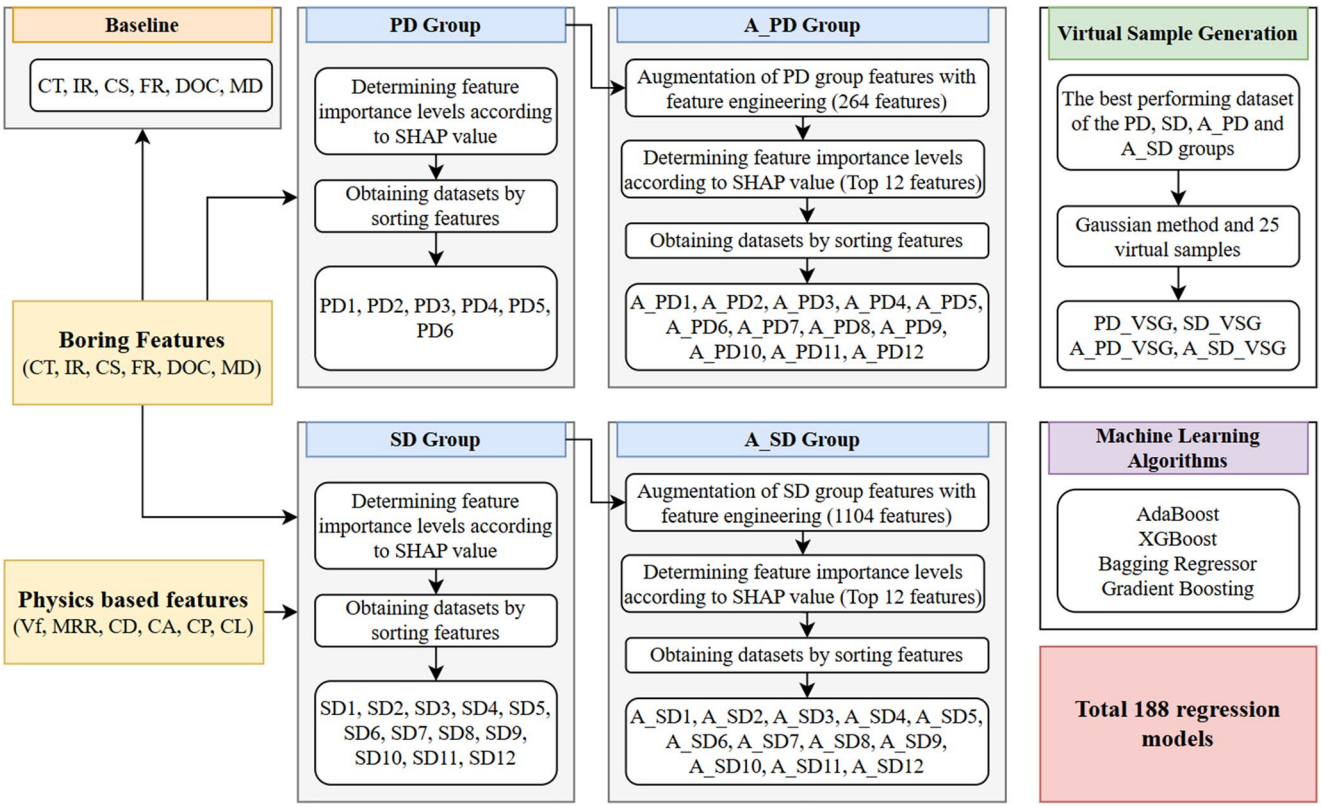


Fig. 3 Scheme of the stages of preparing datasets

A_PD, and the expanded version of the SD dataset was labeled as A_SD.

First, a baseline dataset was prepared in which six boring features were directly considered for the prediction of boring surface roughness. Then, various operations were performed on this dataset, and a group coded with PD, which is the abbreviation of principle dataset, was created. In addition to increasing the predictability of ML models, the explainability of these models is also of great importance. In this context, Shapley Additive Explanations (SHAP) stands out as a powerful tool in model explainability [43]. SHAP calculates each input's contribution to the model output using Shapley values developed from game theory. This method is particularly useful for making sense of the results of complex ML models. When SHAP is employed to explain the effect of model inputs on surface roughness prediction, it can clearly show which inputs have the most impact on the prediction. This increases the reliability of the model and makes the logic behind the predictions more understandable. SHAP values between the six input features and the output response are visualized in Fig. 4. Datasets were constructed by including a single feature at each stage based on the priority levels and rankings. According to the created datasets, models were established, and boring surface roughness prediction performances were calculated and compared. According to the importance level, the features were ranked as CS, CT, FR, IR, DOC, and MD. For example, while the first two features CS and CT were determined for the PD2 model, CS, CT, FR, IR, and DOC features were taken into account for PD5. The in-hole surface roughness was determined as the output prediction value. 50 data points were used for model training and 22 for testing.

For the second group, in addition to the existing six boring parameters, six more physics-based features were added. These added features are penetration rate (Vf), material removal rate (MRR), cutting duration (CD), chip area (CA), chip perimeter (CP), and cutting contact length (CL). These features have a direct effect on the cutting forces, and some of them were used in the analytical modeling of boring forces [4, 5]. For example, the MRR value was calculated using the classical formula using cutting speed, feed rate, and depth of cut. Cutting time was determined by considering feed length and feed rate. Chip area, chip perimeter, and cutting contact length were estimated using geometric models based on tool-workpiece interaction. The accuracy of these physics-based parameters was verified by comparing them with both experimental observations and theoretical expectations. This gave physical recognition to the metal removal process, enhancing the model's explanatory power. Since the cutting forces directly affect the surface roughness values, the mentioned features are determined as physics-based features. In this study, six boring parameters and six physics-based features were combined to obtain twelve features. This group obtained was coded with the letters SD, meaning the second dataset. As in the PD group, 12 features were ranked according to the SHAP value. Figure 5 shows the priority levels and feature rankings for the SD group. Twelve datasets were obtained, with one feature added each time according to the importance level from SD1 to SD12.

To create the third and fourth groups, the dimensionality of the features in the PD6 and SD12 datasets was increased through feature engineering. This process was done to establish models with higher accuracy, reveal complex relationships, and discover stronger features. a, $a^{1/2}$, a^2, a^3, and log (1 + a) functions were used to expand the dimensionality of the features and identify the best characteristics. Every input attribute is designated as a, and combinations of them are computed to produce high-dimensional features. The physical rationale behind these transformations lies in the fact that key factors influencing surface quality during machining—such as energy input, material deformation, and tool–workpiece contact—typically exhibit

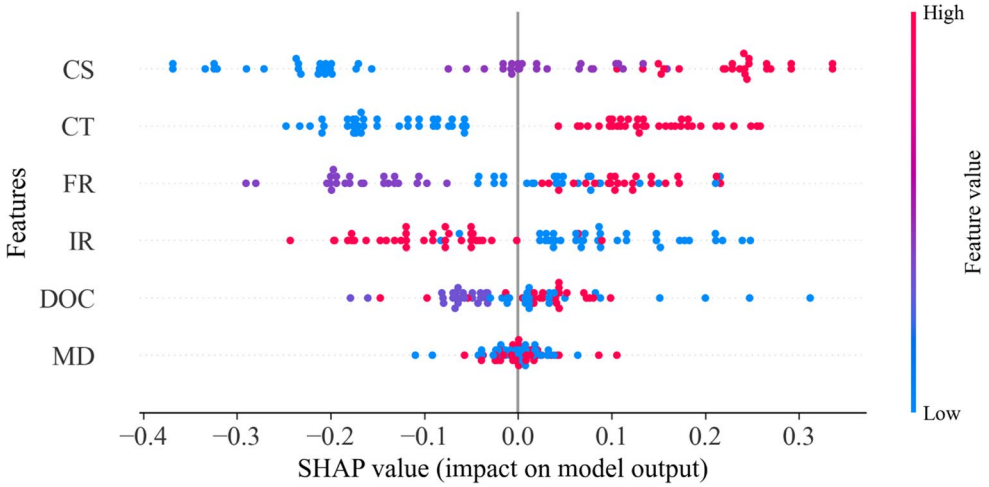


Fig. 4 PD group SHAP values and importance ranking

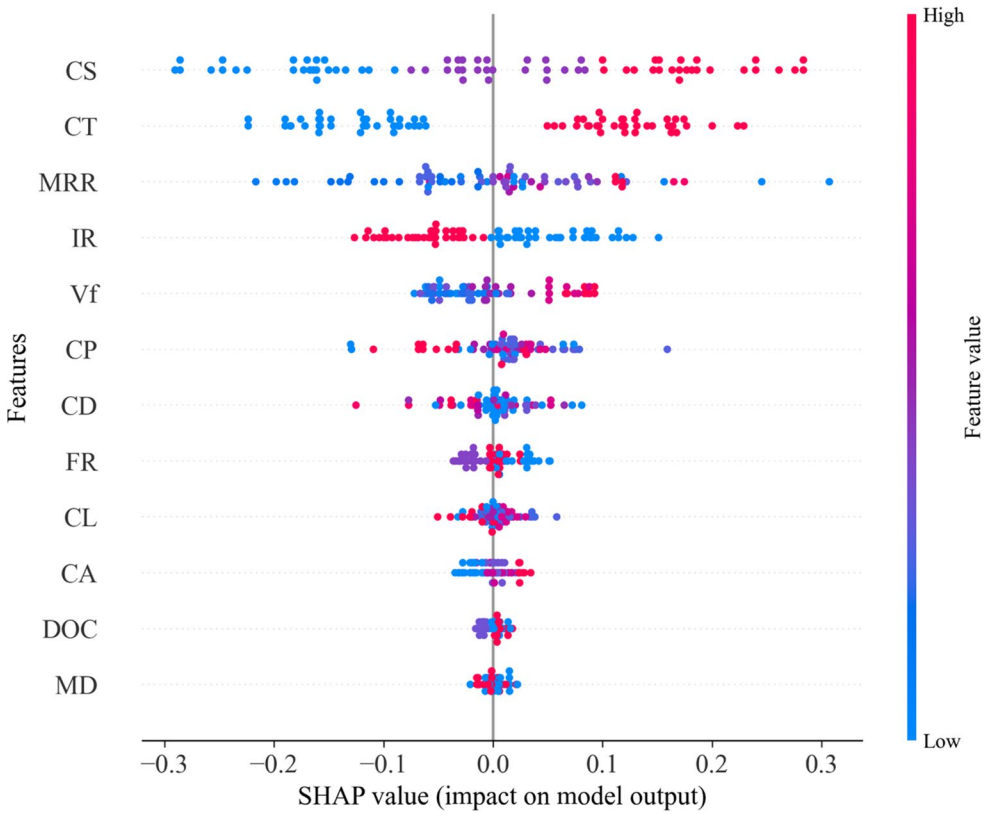


Fig. 5 SD group SHAP values and importance ranking

Table 5 Top twelve features and their importance ratings for the A_PD group

Code	Descriptor	Rank	Code	Descriptor	Rank
P30	$CS^3\sqrt{CT}$	1	P113	$\log(1+FR)\sqrt{IR}$	7
P31	$CS^2\sqrt{CT}$	2	P146	$IR^2\sqrt{DOC}$	8
P159	$\log(1+IR)\,FR^3$	3	P144	$\log(1+FR)\,IR^3$	9
P164	$\log(1+IR)\,FR^2$	4	P128	$\log(1+IR)\,CS^2$	10
P158	$\sqrt{IR}\sqrt{DOC}$	5	P112	$\log(1+IR)\,\log(1+DOC)$	11
P154	$\log(1+FR)\,IR^2$	6	P129	$IR^3\,DOC^2$	12

Table 6 Top twelve features and their importance ratings for the A_SD group

Code	Descriptor	Rank	Code	Descriptor	Rank
S54	$CS^2\sqrt{CT}$	1	S114	$CT^2\,Vf^2$	7
S55	$CS^3\sqrt{CT}$	2	S69	$\sqrt{CT}\sqrt{Vf}$	8
S365	$\log(1+IR)\sqrt{MRR}$	3	S1096	$\log(1+CL)\,CP^2$	9
S368	$\log(1+IR)\,\log(1+MRR)$	4	S378	$\log(1+IR)\,CP^2$	10
S362	$\log(1+IR)\,Vf^2$	5	S347	$\log(1+IR)\,CS^3$	11
S437	$CS^2\sqrt{MRR}$	6	S351	$\log(1+IR)\,FR^3$	12

nonlinear interactions. The impact of the newly engineered features on model accuracy was systematically assessed through feature importance rankings and their effect on prediction performance. Features that demonstrated a substantial contribution to model improvement were prioritized in the final model structure. This technique provided 264 features for PD6 and 1104 features for SD12. These attributes were sorted in order of importance based on SHAP values. The abbreviations A_PD were determined for the new group obtained by increasing the PD group, and A_SD were determined for the new group obtained by increasing the SD group. The listed features are given in Table 5 for A_PD and Table 6 for A_SD. For clarity, the "Code" column in the tables represents the numbering of the new features generated through the feature engineering process. The "Descriptor" column explains the original parameters and mathematical formulas used to derive each new feature. This representation increases the traceability of the derived variables and ensures transparency of the modeling process. SHAP values are given in Fig. 6. In these new groups, 12 ordered datasets were created according to the SHAP value.

3.2 Virtual Sampling Methods

The datasets prepared for boring surface roughness estimation are divided into two parts as training and test sets. It is aimed to increase modeling success and obtain higher precision estimation performance. Especially in machining operations such as boring, it is not possible to conduct many

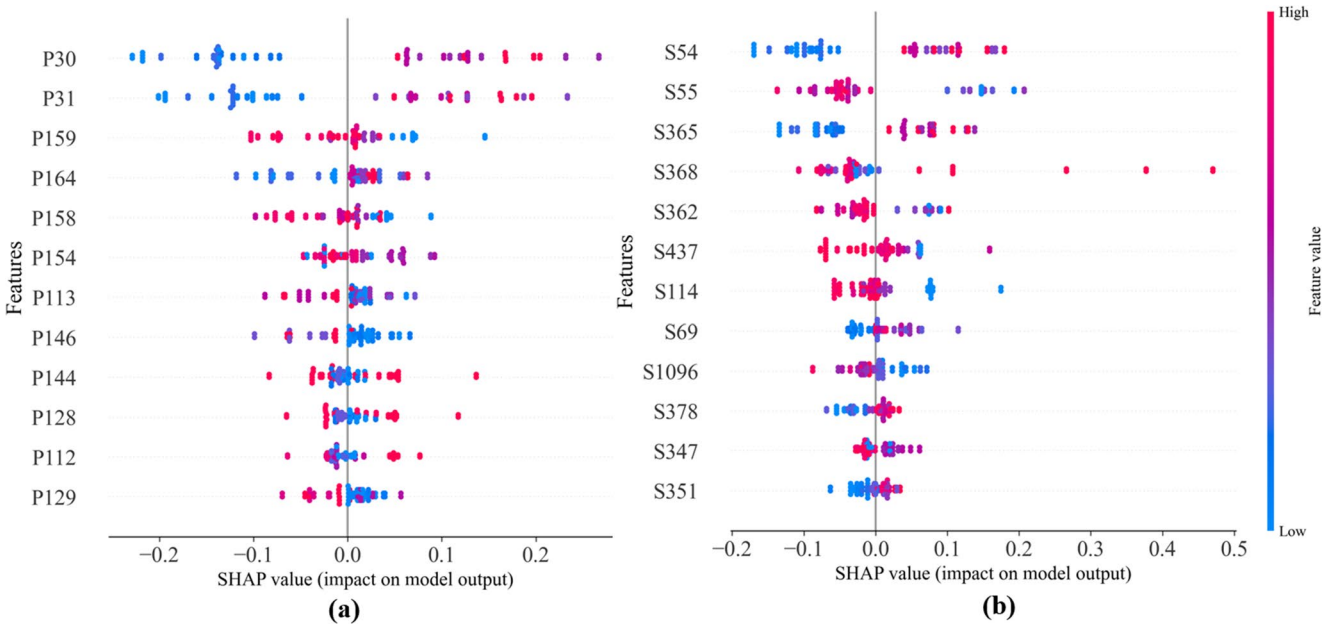


Fig. 6 SHAP values and their importance rankings **(a)** A_PD; **(b)** A_SD

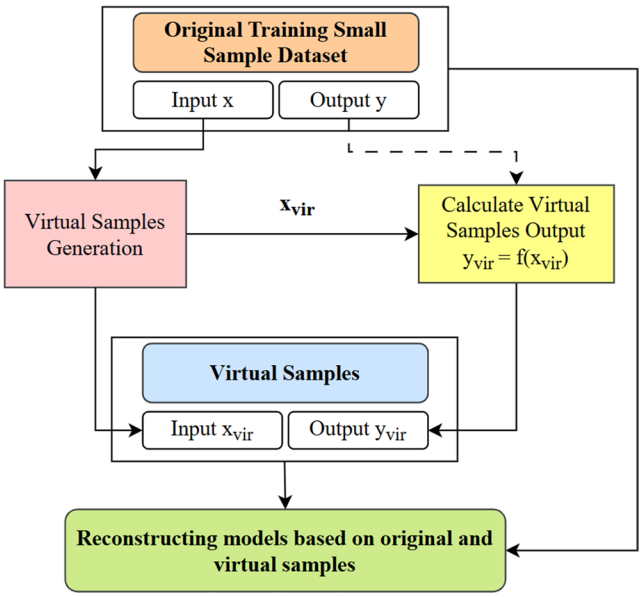


Fig. 7 Flowchart of virtual sample generation

experiments due to time and cost limitations. This situation causes small sampling problems in the establishment of models and estimation performance, especially by using artificial intelligence-supported methods. This situation causes overfitting and non-generalizable models and poor estimation performance [12]. To overcome this situation, virtual samples are added to the training sets with the help of existing data points [29]. Added virtual samples generally improve modeling success and therefore estimation performance. The Gaussian method was used to create virtual samples. Gaussian virtual sample generation is a method of creating new data points based on normal distribution [44]. In this method, the data is assumed to be normally (or Gaussian) distributed around a certain mean and standard deviation. In a Gaussian distribution, the majority of the data is usually concentrated around the mean value, while extreme values are less frequent. The flowchart for creating a virtual sample is given in Fig. 7.

A Gradient boosting algorithm was preferred for estimating the output values of the created virtual samples. This algorithm was preferred because it provided the highest performance increase. 50% of the data, i.e., 25 virtual samples, were added to the training set. Due to the high cost, time, and labor associated with machining experiments, the dataset used in this study is limited in size; therefore, virtual sampling was employed to augment the training data, with the number of virtual samples carefully limited to 50% of the original training set to preserve the dataset's natural distribution. Virtual samples were applied to the best-performing datasets of the PD, SD, A_PD, and A_SD groups.

4 Performance Evaluation Metrics

Of the 72 data points, 50 were used for training and 22 for testing. The test estimations and actual values produced by the founded models were assessed by metrics. This research

employed MAPE, MSE, and MAE measures to compare the models' performance. Performance measures were determined to strongly compare the real and estimated values of the boring surface roughness. Generally, the smaller the MAPE, MSE, and MAE values, the better. Equations 1, 2, 3, and 4 include formulas for performance measures. While the MSE, MAE, and R^2 formulas are taken from source [6], the MAPE calculation is taken from source [12]. The number of each sample (n), actual outcomes (ti), the mean of the actual values ($\bar{t}_i$), and predicted outcomes (yi) are represented.

$$\mathrm{MSE} = \frac{1}{n}\sum_{i=1}^{n}(t_i - y_i)^2 \tag{1}$$

$$\mathrm{MAE} = \frac{1}{n}\sum_{i=1}^{n}|t_i - y_i| \tag{2}$$

$$R^2 = 1 - \frac{\sum_{i=1}^{n}(t_i - y_i)^2}{\sum_{i=1}^{n}\left(t_i - \bar{t}_i\right)^2} \tag{3}$$

$$\mathrm{MAPE} = \frac{1}{n}\sum_{i=1}^{n}\frac{|t_i - y_i|}{t_i} \tag{4}$$

5 Results and Discussion

This study aims to successfully model and predict the surface roughness induced by the boring process of 1.2738 workpieces on a milling machine. Boring operation is heavily preferred in workpieces where high-quality holes are desired. Various negative situations may occur due to the fact that the process takes place inside the hole, the boring bar is long and weak, centrifugal forces, and dynamic rigidities. These negativities cause variable results in surface quality. To overcome these problems, the input features need to be optimized. This can be achieved by preprocessing modeling and estimation of surface roughness. Variables such as radial cutting depth, feed, speed, cutting insert radius, and cutter coating are very important for the success of the boring process. Therefore, it is necessary to carefully determine and optimize these values for the health of surface roughness.

Figure 8 illustrates how boring parameters affect surface roughness. As clearly seen in Fig. 8a, small cutting-edge radius produces higher roughness values. A smaller nose radius has a smaller contact area and causes more surface feed marks [45]. According to Fig. 8b, while the increase in cutting speed directly increases the surface roughness, it has a parabolic effect with the feed rate, and the roughness values are more optimized at medium feed rate values. Since higher cutting speeds cause more cutter rotation per unit time, vibrations may have increased as a result of dynamic rigidity [46]. This situation has negatively affected the surface roughness. In Fig. 8c, while increasing the depth of cut grows the roughness value, the roughness improves slightly near the hole exit. As the depth of cut grows, so does the volume of chips removed per unit of time. This circumstance may have raised the cutting forces, resulting in more surface roughness [10]. The correlation between boring parameters and physics-based features is visualized in Fig. 8d. In addition, the relationship between all features and surface roughness is given. The highest positive correlation with surface roughness is cutting speed, the highest negative correlation is cutting edge radius, and the lowest correlation is contact length. The highest correlation between surface roughness and boring parameters is cutting speed, and the highest negative correlation is penetration speed for physics-based features. The highest positive correlation between boring parameters and physics-based features is between radial depth of cut and chip perimeter, and the highest negative correlation is between roughness measurement distance and cutting time. While the penetration rate, material removal rate, and chip area from physics-based features are highly correlated with feed rate, contact length, chip area, chip perimeter, and the material removal rate are highly correlated with radial depth of cut.

Since surface roughness is directly related to output responses such as tool wear, cutting forces, and cutting parameters, advanced methods are needed for effective modeling [47]. Modeling a large number of input features linearly can result in estimates that do not approximate the true values [48]. Therefore, models that better understand the complex relationship and patterns between input features and surface roughness and can make meaningful inferences and predictions are required. The important point here is to determine the input features that can increase the success of surface roughness prediction and give better results. For this purpose, input features can be used directly, features are ranked according to their importance, physics-based features are added, the dimensionality of the features is increased, or virtual samples are produced. It is useful to examine in depth and comparatively how these methods will affect datasets with small samples. Furthermore, this study intended to determine the impact of several ML methods on the accuracy of boring surface roughness prediction.

Adaboost, XGBoost, Bagging regressor, and Gradient boosting algorithms were used to effectively model the

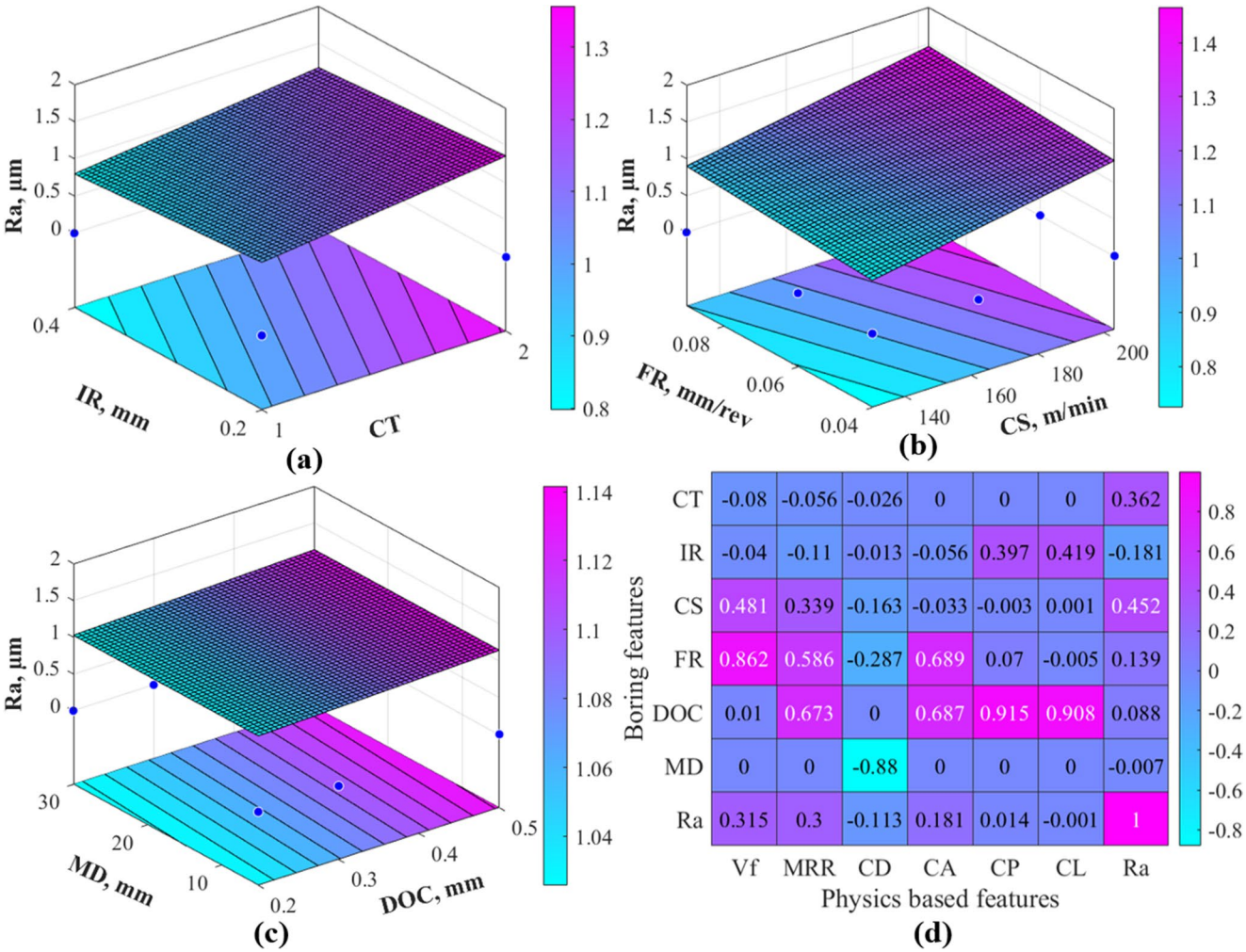


Fig. 8 Relationship of input features with surface roughness **(a)** CT-IR; **(b)** CS-FR; **(c)** DOC-MD; **(d)** correlation values

Table 7 Performance metrics by algorithm for the baseline

Algorithms	MAE	MSE	MAPE	R^2
AB	0.249	0.108	0.346	0.589
XGB	0.253	0.131	0.323	0.576
BR	0.267	0.175	0.408	0.402
GB	0.285	0.152	0.421	0.480

surface roughness resulting from the precision boring process of the 1.2738 workpiece on the milling machine. The estimation performances obtained with ML algorithms for the baseline dataset are given in Table 7. According to the MAPE value, the best performance was obtained with XGB, while the worst performance was obtained with the GB algorithm. However, when the R^2 values are examined, it is clear that the established model cannot achieve the desired success and that its performance needs to be improved by using various ML methods. In order to increase the performance success, dataset groups were created with various methods and examined in depth in the following sections.

The performance parameters of the test datasets were rigorously studied to be evaluated using the models shown in Fig. 9. In general, the performance metrics tend to decrease as the number of attributes in the dataset increases. However, once the optimal number of attributes is reached, performance metrics climb again. ML algorithms showed different performances according to the changing number of features. These results are compatible with the literature and are quite necessary in terms of determining the features that provide optimum performance [11]. Because the optimum features and feature sizes vary according to the feature group and dataset. While the optimum feature numbers for the PD and SD groups show a more distinct peak, the optimum feature numbers for the A_PD and A_SD groups obtained after increasing the feature size are a little closer to each other. It was evaluated that such a situation occurred because the first 12 features with the highest performance were selected after increasing the feature size while all features were taken into account for PD and SD.

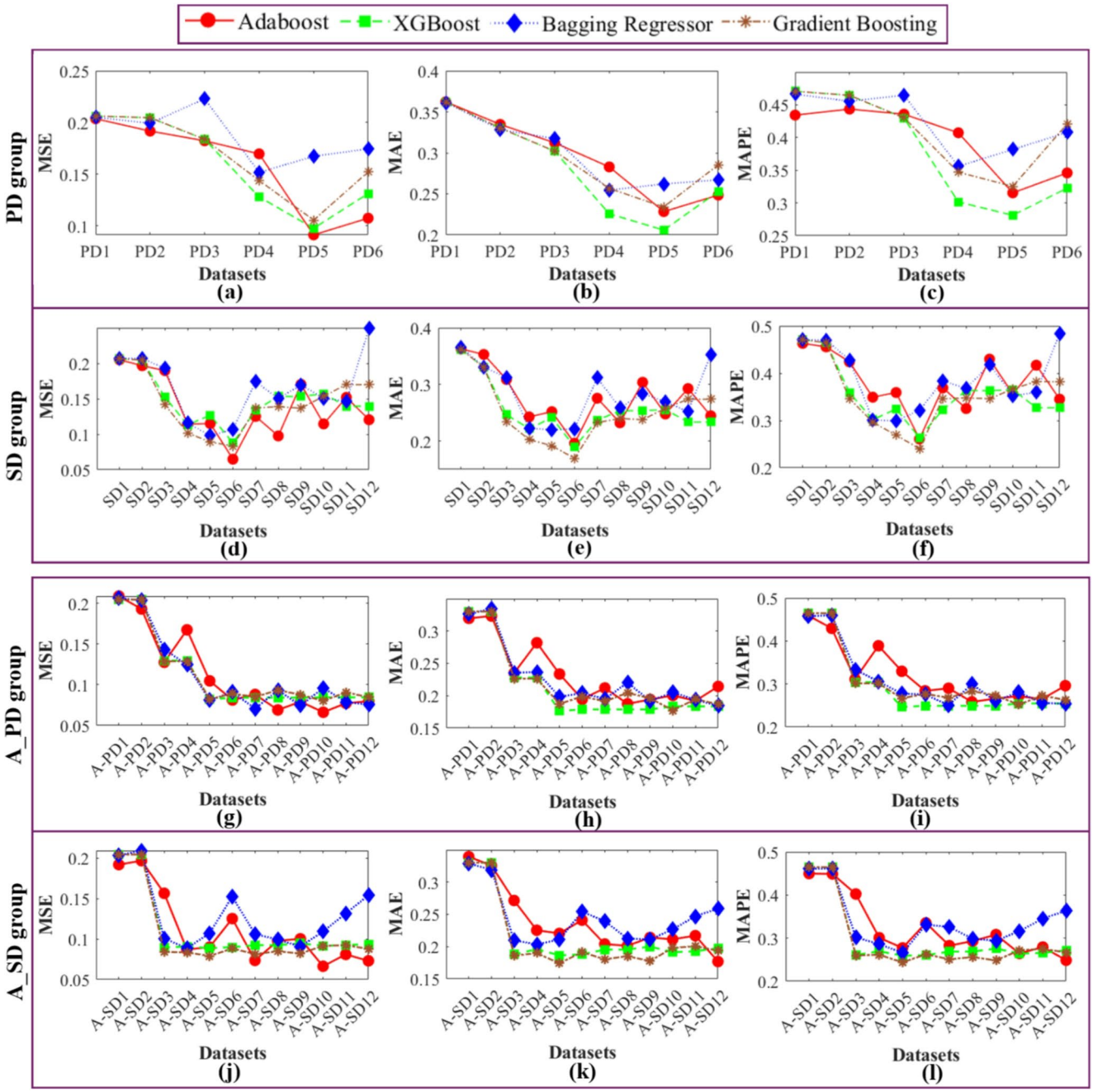


Fig. 9 Performance metrics of the created groups **(a-d-g-j)** MSE; **(b-e-h-k)** MAE; **(c-f-i-l)** MAPE

Optimum feature sizes and performance criteria according to dataset groups and algorithms are given in Table 8. Datasets with 6 features for the SD group and 5 features for the other groups provided the calculation of optimum performance metrics. According to MAPE values, the highest performance success was obtained with XGB algorithms for PD and A_PD groups GB algorithms for SD and A_SD groups. The lowest MAPE value was obtained with the SD6 model and GB algorithm, while the highest MAPE value was obtained with the PD4 model and BR algorithm. When R^2 values are examined, performance success for all algorithms increased by optimizing and augmenting feature dimensions compared to the baseline model.

The MAPE performance change in the dataset groups according to the ML algorithms is shown in Fig. 10. The models with the highest performing feature numbers in the dataset groups were taken into account. The PD group is represented by PD5, the SD group by SD6, the A_PD group

Table 8 Optimal feature sizes and performance criteria according to dataset groups and algorithms

Groups	Algorithms	Optimal feature dimension	MAE	MSE	MAPE	R^2
PD	AB	PD5	0.228	0.091	0.315	0.644
	XGB	PD5	0.206	0.098	0.281	0.662
	BR	PD4	0.255	0.152	0.356	0.452
	GB	PD5	0.234	0.106	0.325	0.612
SD	AB	SD6	0.196	0.065	0.261	0.749
	XGB	SD6	0.190	0.088	0.264	0.673
	BR	SD5	0.220	0.098	0.299	0.617
	GB	SD6	0.169	0.083	0.240	0.681
A_PD	AB	A_PD8	0.188	0.069	0.258	0.730
	XGB	A_PD5	0.176	0.082	0.246	0.695
	BR	A_PD7	0.195	0.071	0.251	0.745
	GB	A_PD10	0.177	0.080	0.252	0.693
A_SD	AB	A_SD12	0.177	0.073	0.249	0.714
	XGB	A_SD5	0.187	0.089	0.259	0.675
	BR	A_SD5	0.211	0.107	0.266	0.600
	GB	A_SD5	0.174	0.079	0.244	0.703

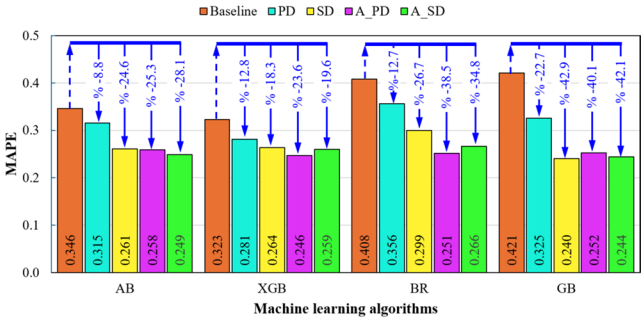


Fig. 10 Performance changes in dataset groups according to ML algorithms

by A_PD5, and the A_SD group by A_SD5 models. According to the figure, instead of using the normal input features directly, determining the upper-level features according to the importance level, adding physics-based features, or increasing the feature size contribute significantly to the prediction performance. While the lowest performance increase was obtained with the Adaboost algorithm and PD, the highest performance increase was obtained with the Gradient boosting algorithm and SD. By ranking the features in the baseline dataset according to their importance and then using the top performing features, a performance increase of 8.8–22.7% occurred for the PD group obtained. While a performance increase between 18.3% and 42.9% occurred for the SD group obtained by adding physics-based features to the boring features, a performance increase between 23.6% and 40.1% occurred for the A_PD group obtained by increasing the feature size. After adding physics-based features, a performance increase between 19.6% and 42.1% occurred for the A_SD group obtained by increasing the feature size. In a study to predict the surface roughness of the workpiece manufactured by the selective laser melting process, random forests, artificial neural networks, support vector machines, and Bayesian networks were employed [32]. With the addition of physics-based features, the performance deteriorated by 1.1% in SVM, while the performance improved by 35.9% in ANN. Increasing the feature size yielded a performance increase of 12.1–40.4% while using both methods yielded a performance increase of 13.8–49.8%. Compared to the current study, the results obtained are quite sufficient and acceptable.

Recently, virtual samples have been added to training sets to overcome small sampling problems and to increase prediction performance. When the literature is examined, the prediction performance of the output responses generally improves in this way. Since virtual samples are added according to the data points in the existing training set, complex relationships and patterns in the dataset can be well represented. Especially in regions where data is sparse, virtual samples added to the training set make significant contributions to obtaining more generalizable predictions [49]. In the current research, to examine the impact of adding virtual samples on the prediction performance, 25 virtual samples, which are 50% of the training set, were added to the training set. The Gaussian virtual sample generation method was used to create virtual input features. The output responses of the generated virtual input features were estimated with the gradient boosting algorithm, which showed the highest performance increase. The obtained virtual data points were added to the training set, and the models were trained, and performance metrics were calculated with fixed test sets.

Figure 11 shows the real data points and the added virtual sample points. The added virtual samples are in the regions where the data in the training set is sparse and on the optimal line. The distributions of the produced virtual samples

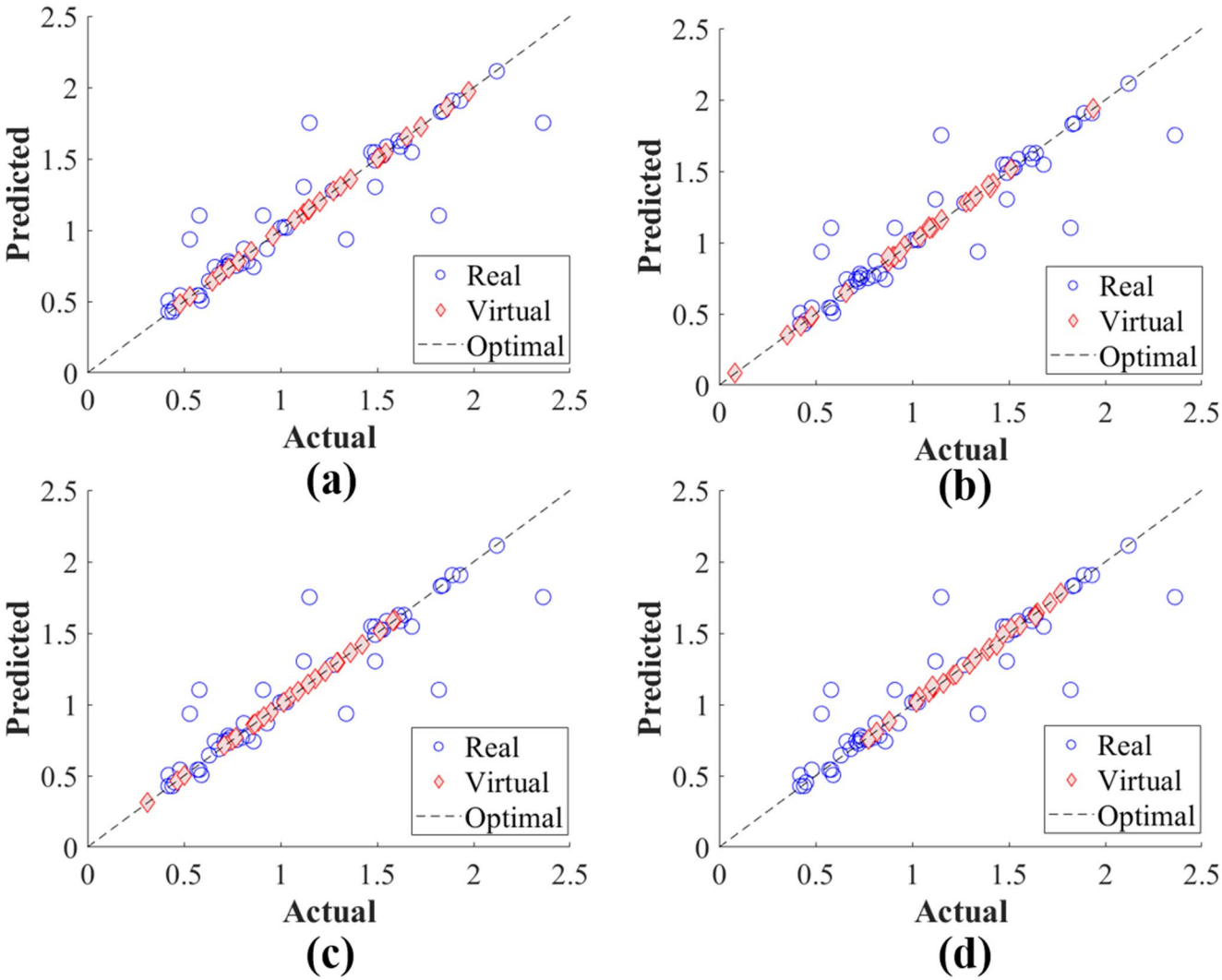


Fig. 11 Virtual data points added to real data points **(a)** PD5; **(b)** SD6; **(c)** A_PD5; **(d)** A_SD5

Table 9 Prediction performance metrics of the datasets determined after the virtual sample was added to the training set

Dataset	Optimal algorithm	MAE	MSE	MAPE	R^2
PD	BR	0.197	0.089	0.267	0.659
SD	GB	0.167	0.079	0.237	0.697
A_PD	BR	0.185	0.071	0.246	0.736
A_SD	GB	0.169	0.073	0.237	0.721

vary according to the dataset and feature numbers used. It can be said that the obtained virtual samples have a sufficient distribution in the regions where the data is sparse.

The performance metrics obtained after adding virtual samples are given in Table 9. The algorithm with the lowest MAPE value, i.e., the highest performance, was found to be GB. Secondly, the BR algorithm was determined. SD and A_SD datasets provided higher performance success. Augmenting the data according to R^2 values played an important role in increasing the performance success.

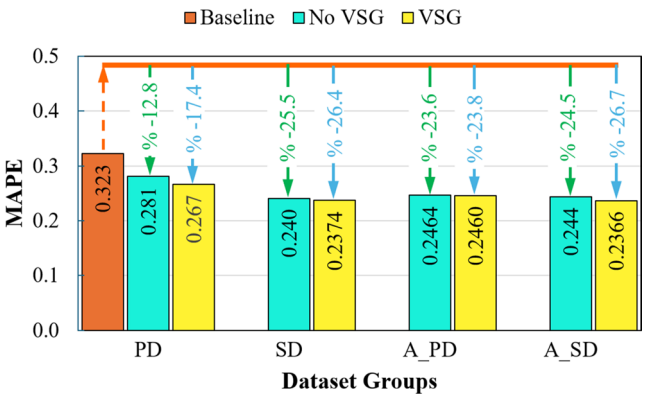


Fig. 12 Performance change of established models compared to the initial ones

Figure 12 depicts the change in MAPE performance between the established models and the initial one. The model obtained when the boring features are used directly

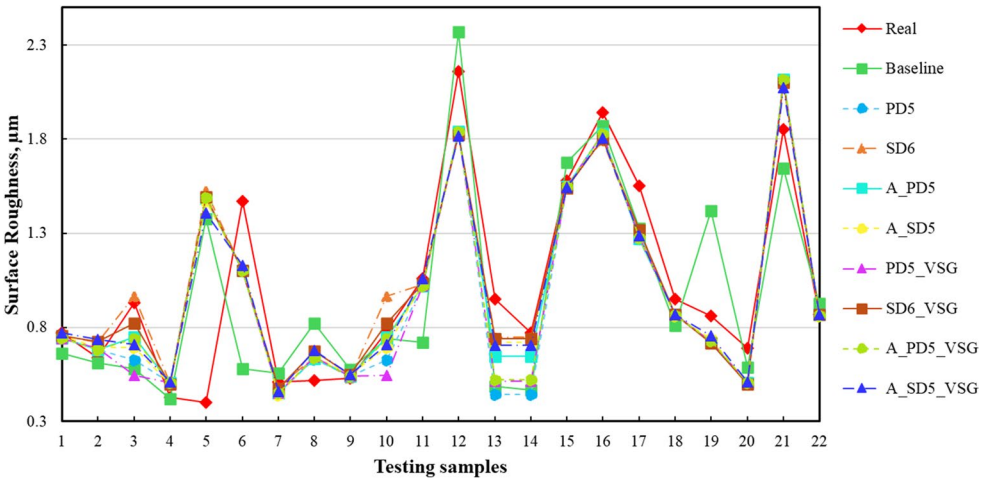


Fig. 13 Trends of boring surface roughness of the established models for the test set points

without any processing is given as the baseline in the figure. By applying different ML methods to the initial dataset, their contributions to the boring surface roughness prediction performance were examined in depth and compared. By sorting the boring parameters according to the SHAP value and using the first five features as input, a 12.8% decrease in the MAPE value occurred. When virtual samples were added to the dataset with the first five features, a performance increase of 17.4% occurred. After adding physics-based features to the baseline dataset, the first six features ranked according to SHAP value provided a performance increase of 25.5%, while the addition of virtual samples provided a performance increase of 26.4%. For PD and SD datasets, increasing the features and sorting them according to SHAP value increased the performance by 23.6% and 24.5% compared to the baseline, respectively, while adding virtual samples increased the performance by 23.8% and 26.7%, respectively. Compared to the 23.8% performance increase obtained in a study [50], the performance increase achieved is at a quite acceptable level.

In Fig. 13, the predictions of the test set points by the established models are visualized. In general, the boring surface roughness can be predicted successfully with the help of the established models. The model that showed the highest prediction performance was A_SD5_VSG. The virtual samples added to the training set caused a significant improvement in the prediction performance.

As a result, the A_SD5_VSG integrated model delivered the best performance results. There was a performance increase of approximately 27% compared to the baseline dataset. In order to obtain this integrated model, firstly physics-based features were added to the boring features. Then the size of the obtained features was increased. Then, the integrated model was obtained by adding virtual samples to the first five features ranked according to the SHAP value.

6 Conclusion

This study aims to deeply analyze the consequences of various techniques such as ranking the features according to their importance, adding physics-based features, increasing the feature size, and generating virtual samples on the prediction performance in order to make high-precision boring surface roughness predictions and overcome small sampling problems. With the proposed method, input features can be optimized to obtain the desired surface roughness before the boring process. Thus, efficient, more precise, and cost-effective process planning can be realized. The key findings from the study are presented below.

1) Surface roughness rises with higher levels of depth of cut and cutting speed. Among the boring features, the feature with the highest correlation with surface roughness and the highest SHAP value is the cutting speed, while in terms of physics-based features, it is the penetration rate.
2) When compared to the baseline dataset, the PD group and the AB algorithm showed the smallest performance increase, while the SD group and the GB algorithm showed the greatest increase.
3) The highest performance increase for the AB algorithm was in the A_SD group; for the XGB and BR algorithms, the A_PD group; for the GB algorithm, the SD group produced the highest performance increase compared to MAPE. Therefore, each algorithm showed different performance according to the features in the dataset.

4) When the contribution of virtual sample generation is examined, a performance increase of 17.4% for PD_VSG, 26.4% for SD_VSG, 23.8% for A_PD_VSG, and 26.7% for A_SD_VSG occurred compared to the baseline dataset.
5) As a result, the A_SD5_VSG integrated model generated the best performance results. There was a performance increase of approximately 27% compared to the baseline dataset. In order to obtain this integrated model, firstly physics-based features were added to the boring features. Then the size of the obtained features was increased. Then, the integrated model was obtained by adding virtual samples to the first five features ranked according to the SHAP value.

In future studies, it would be useful to examine and compare different methods for solving the small sampling problem. In addition, different algorithms and virtual sampling generation methods can be examined.

Acknowledgements The Gazi University Scientific Research Projects Unit funded this project with grant number 07/2011-70. The researchers appreciate the help offered by Gazi University's BAP department.

Author contributions Aslan Akdulum: methodology, formal analysis and investigation, writing-original draft preparation, writing-review and editing, resources, software, data curation.
Yunus Kayır: conceptualization, methodology, formal analysis and investigation, writing, review and editing, funding acquisition.

Funding The Gazi University Scientific Research Projects Unit funded this project with grant number 07/2011-70.

Data Availability Data will be shared upon reasonable request.

Declarations

Competing Interest The authors declare to have no known competing financial interests or personal relationships that could have influenced the research presented in this study.

References

1. Senbabaoglu, F., Lazoglu, I., & Ozkeser, S. O. (2010). Experimental analysis of boring process on automotive engine cylinders. *The International Journal of Advanced Manufacturing Technology*, *48*, 11–21. https://doi.org/10.1007/s00170-009-2271-9
2. Zhang, G., & Kapoor, S. (1987). Dynamic modeling and analysis of the boring machining system. *Journal of Manufacturing Science and Engineering*, *109*(3), 219–226. https://doi.org/10.1115/1.3187122
3. Subramani, G., Kapoor, S., & DeVor, R. (1993). A model for the prediction of bore cylindricity during machining. *Journal of Manufacturing Science and Engineering*, *115*(1), 15–22. https://doi.org/10.1115/1.2901630
4. Atabey, F., Lazoglu, I., & Altintas, Y. (2003). Mechanics of boring processes—Part I. *International Journal of Machine Tools and Manufacture*, *43*(5), 463–476. https://doi.org/10.1016/S0890-6955(02)00276-6
5. Atabey, F., Lazoglu, I., & Altintas, Y. (2003). Mechanics of boring processes—Part II—multi-insert boring heads. *International Journal of Machine Tools and Manufacture*, *43*(5), 477–484. https://doi.org/10.1016/S0890-6955(02)00277-8
6. Akdulum, A., Süzgünol, M., & Kayir, Y. (2024). Prediction of feed force with machine learning algorithms in boring of AISI P20 plastic mold steel. *Materials Today Communications*, *41*(110704), 1–17. https://doi.org/10.1016/j.mtcomm.2024.110704
7. Kuster, F., & Gygax, P. (1990). Cutting dynamics and stability of boring bars. *CIRP Annals*, *39*(1), 361–366. https://doi.org/10.1016/S0007-8506(07)61073-7
8. Kaliński, K. J., Galewski, M. A., Mazur, M. R., & Stawicka-Morawska, N. (2021). An improved method of minimizing tool vibration during boring holes in large-size structures. *Materials*, *14*(16), 4491. https://doi.org/10.3390/ma14164491
9. Liu, C., Ren, J., Zhang, Y., & Shi, K. (2023). The effect of tool structure and milling parameters on the milling quality of CFRP based on 3D surface roughness. *International Journal of Precision Engineering and Manufacturing*, *24*(6), 931–944.
10. Akdulum, A., & Kayir, Y. (2024). Experimental comparison of the indexable drilling with different U drills on hole quality. *Machining Science and Technology*, *28*(1), 1–28. https://doi.org/10.1080/10910344.2023.2286658
11. Siyambaş, Y., & Akdulum, A. (2024). Prediction of surface roughness using different features in vortex cooled turning process of Ti6Al4V alloy. *Measurement*. 115258. https://doi.org/10.1016/j.measurement.2024.115258
12. Tian, W., Zhang, J., Zhao, F., Feng, X., Mei, X., Chen, G., & Wang, H. (2024). Interpolation-based virtual sample generation for surface roughness prediction. *Journal of Intelligent Manufacturing*, *35*(1), 343–353. https://doi.org/10.1007/s10845-022-02054-4
13. Zhang, R., Lv, D., & Wang, Y. (2021). Wear performance and mechanisms of PCBN tools in boring of powder metallurgy steels. *The International Journal of Advanced Manufacturing Technology*, *114*(11), 3605–3614. https://doi.org/10.1007/s00170-021-07136-w
14. Veiga, F., Del Val, G., Penalva, A., Pereira, M. L., & Suárez, O. (2021). Predicted torque model in low-frequency-assisted boring (lfab) operations. *Metals*, *11*(7), 1009. https://doi.org/10.3390/met11071009. & López de Lacalle Marcaide, L. N.
15. Morelo, F., Grabarski, M. I., de Camargo Beltrão, P. A., & Pintaude, G. (2017). Surface integrity of bored super duplex stainless steel SAF 2507. *Journal of the Brazilian Society of Mechanical Sciences and Engineering*, *39*, 2649–2658. https://doi.org/10.1007/s40430-016-0642-3
16. Zhan, Y., Zhou, J., Zuo, Z., Xu, Y., Li, X., & Jia, M. (2022). Multi-index cutting parameters optimization for surface quality and cutting energy consumption of boring. *Métodos Numéricos Para Cálculo Y Diseño En Ingeniería: Revista Internacional*, *38*(1), 1–18. https://doi.org/10.23967/j.rimni.2022.03.004

17. Thasana, W., Sugimura, N., Iwamura, K., & Tanimizu, Y. (2014). A study on Estimation of 3-dimensional surface roughness of boring processes including kinematic motion deviations. *Journal of Advanced Mechanical Design Systems and Manufacturing*, *8*(4), 1–12. https://doi.org/10.1299/jamdsm.2014jamdsm0046
18. Zheng, Z., Guo, J., Gao, R., Jin, X., Jiang, Z., & Li, C. (2022). Research on process simulation and surface quality of the thin-walled neck by precision boring. *The International Journal of Advanced Manufacturing Technology*, *123*(11), 4009–4024. https://doi.org/10.1007/s00170-022-10541-4
19. Yang, R. T., Liao, H. T., Yang, Y. K., & Lin, S. S. (2012). Modeling and optimization in precise boring processes for aluminum alloy 6061T6 components. *International Journal of Precision Engineering and Manufacturing*, *13*, 11–16. https://doi.org/10.1007/s12541-012-0002-x
20. Akman, M., Uçar, M., Uçar, Z., Uçar, K., Baraklı, B., & Bozkurt, M. (2022). Determination of body fat percentage by gender based with photoplethysmography signal using machine learning algorithm. *IRBM*, *43*(3), 169–186. https://doi.org/10.1016/j.irbm.2020.12.003
21. Kim, H., Lee, S., Lee, J., Park, K. H., & Nam, S. (2025). Enhancing tool wear prediction accuracy by integrating Multi-Task learning with cutting force Estimation. *International Journal of Precision Engineering and Manufacturing-Green Technology*. 1–21.
22. Akdulum, A., & Kayir, Y. (2023). Modeling and estimation of thrust force, torque, and surface roughness in indexable drilling of AA6061-T651 with Taguchi, ANN, and ANFIS. *Sādhanā*. 48(3): 143. https://doi.org/10.1007/s12046-023-02209-w
23. Nguyen, V. H., & Le, T. T. (2024). Predicting surface roughness in machining aluminum alloys taking into account material properties. *International Journal of Computer Integrated Manufacturing*, 1–22. https://doi.org/10.1080/0951192X.2024.2372252
24. Kim, J. W., Nam, J., Kim, G. Y., & Lee, S. W. (2023). Artificial intelligence (AI)–based surface quality prediction model for carbon fiber reinforced plastics (CFRP) milling process. *International Journal of Precision Engineering and Manufacturing-Smart Technology*, *1*(1), 35–47.
25. Siyambaş, Y., Akdulum, A., Çakıroğlu, R., & Uzun, G. (2025). Estimation of cutting temperature using machine learning based on signal information received from power analyzer in vortex machining conditions. *Journal of Manufacturing Processes*, *137*, 100–112. https://doi.org/10.1016/j.jmapro.2025.02.004
26. Zhao, H., Cao, Y., Sergey, G., Kuzin, V., Du, J., & He, W. (2024). Research on intelligent prediction of surface roughness in cutting 42CrMo steel by using particle swarm optimization-based support vector machine. *International Journal of Precision Engineering and Manufacturing*. 1–15.
27. Peng, C., Qi, J., Zhou, S., Yang, S., Tao, R., Shao, H., & Li, W. (2025). Effect of feature size on defects, microstructure, and mechanical properties of selective laser melted AlSi10Mg lattice structure. *Metals*, *15*(1), 77. https://doi.org/10.3390/met15010077
28. Kaigude, A. R., Khedkar, N. K., Jatti, V. S., Salunkhe, S., Cep, R., & Nasr, E. A. (2024). Surface roughness prediction of AISI D2 tool steel during powder mixed EDM using supervised machine learning. *Scientific Reports*, *14*(1), 9683. https://doi.org/10.1038/s41598-024-60543-3
29. Song, X. L., He, Y. L., Li, X. Y., Zhu, Q. X., & Xu, Y. (2023). Novel virtual sample generation method based on data augmentation and weighted interpolation for soft sensing with small data. *Expert Systems with Applications*, *225*, 120085. https://doi.org/10.1016/j.eswa.2023.120085
30. Zhu, Q. X., Chen, Z. S., Zhang, X. H., Rajabifard, A., Xu, Y., & Chen, Y. Q. (2020). Dealing with small sample size problems in process industry using virtual sample generation: A Kriging-based approach. *Soft Computing*, *24*, 6889–6902. https://doi.org/10.1007/s00500-019-04326-3
31. Akdulum, A., & Kayir, Y. (2023). Prediction of thrust force in indexable drilling of aluminum alloys with machine learning algorithms. *Measurement*, *222*, 113655. https://doi.org/10.1016/j.measurement.2023.113655
32. Wang, H., Li, B., & Xuan, F. Z. (2022). A dimensionally augmented and physics-informed machine learning for quality prediction of additively manufactured high-entropy alloy. *Journal of Materials Processing Technology*, *307*, 117637. https://doi.org/10.1016/j.jmatprotec.2022.117637
33. Seppi, M., Linnosmaa, J., & Zeb, A. Physics-Informed Machine Learning Surrogate Models: Enhancing Data-Driven Forecasting for Digital Twins in Mineral Processing. *Available at SSRN 5124811*. https://doi.org/10.1016/j.mineng.2025.109424
34. Li, B., Zhang, W., & Xuan, F. (2022). Machine-learning prediction of selective laser melting additively manufactured part density by feature-dimension-ascended bayesian network model for process optimisation. *The International Journal of Advanced Manufacturing Technology*, *121*(5), 4023–4038. https://doi.org/10.1007/s00170-022-09555-9
35. Wang, X., Lyu, J., Peter, J. D., Kim, B. G., Parameshachari, B., Li, K., & Wei, W. (2025). Explaining sentiments: Improving explainability in sentiment analysis using local interpretable Model-Agnostic explanations and counterfactual explanations. *IEEE Transactions on Computational Social Systems*. https://doi.org/10.1109/TCSS.2025.3531718
36. Akdulum, A., Süzgünol, M., & Kayır, Y. (1.2738). Malzemesinin Baralanmasında İşleme Parametrelerinin Baralama Torkuna Etkisinin Yanıt Yüzey Yöntemi Ile optimizasyonu. *Manufacturing Technologies and Applications*, *6*(1), 79–88. https://doi.org/10.52795/mateca.1552826
37. Akdulum, A., Süzgünol, M., & Kayır, Y. (2025). AISI P20 Plastik Kalıp Çeliğinin Dik İşleme Tezgahında Baralanmasında İşleme Parametrelerinin Kesme Torkuna Etkisi. *Gazi Üniversitesi Fen Bilimleri Dergisi Part C: Tasarım ve Teknoloji*. 1–1. https://doi.org/10.29109/gujsc.1549251
38. Gologlu, C., & Sakarya, N. (2008). The effects of cutter path strategies on surface roughness of pocket milling of 1.2738 steel based on Taguchi method. *Journal of Materials Processing Technology*, *206*(1–3), 7–15. https://doi.org/10.1016/j.jmatprotec.2007.11.300
39. Mahmood, J., Mustafa, G., & Ali, M. (2022). Accurate Estimation of tool wear levels during milling, drilling and turning operations by designing novel hyperparameter tuned models based on LightGBM and stacking. *Measurement*, *190*, 110722. https://doi.org/10.1016/j.measurement.2022.110722
40. Lavanya, G., Sundaramurthy, K., Makesh, M., & Rajarathnam, D. (2025). Machine learning approach in cutting force prediction and optimization Ff parameters in end milling of aluminum 6063. *Academic Journal of Manufacturing Engineering*, *23*(1). https://doi.org/10.5281/zenodo.15180896
41. Martinez, W., & Gray, J. B. (2016). Noise peeling methods to improve boosting algorithms. *Computational Statistics & Data Analysis*, *93*, 483–497. https://doi.org/10.1016/j.csda.2015.06.010

42. Mihelich, M., Dognin, C., Shu, Y., & Blot, M. (2020). *A characterization of mean squared error for estimator with bagging*. in *International Conference on Artificial Intelligence and Statistics*. https://doi.org/10.48550/arXiv.1908.02718
43. Li, Q., Ji, Y., Zhu, M., Zhu, X., & Sun, L. (2024). Unsupervised feature selection using chronological fitting with Shapley additive explanation (SHAP) for industrial time-series anomaly detection. *Applied Soft Computing*, *155*, 111426. https://doi.org/10.1016/j.asoc.2024.111426
44. Shen, L., & Qian, Q. (2022). A virtual sample generation algorithm supporting machine learning with a small-sample dataset: A case study for rubber materials. *Computational Materials Science*, *211*, 111475. https://doi.org/10.1016/j.commatsci.2022.111475
45. Gökkaya, H., & Nalbant, M. (2007). The effects of cutting tool geometry and processing parameters on the surface roughness of AISI 1030 steel. *Materials & Design*, *28*(2), 717–721. https://doi.org/10.1016/j.matdes.2005.09.013
46. Akdulum, A., & Kayir, Y. (2024). Investigation of deviation from diameter, circularity and cylindricality in drilling AA2024-T351 with U drills with different properties. *Journal of the Faculty of Engineering and Architecture of Gazi University*, *39*(2), 1167–1178. https://doi.org/10.17341/gazimmfd.1136798
47. Cakir, M. C., Ensarioglu, C., & Demirayak, I. (2009). Mathematical modeling of surface roughness for evaluating the effects of cutting parameters and coating material. *Journal of Materials Processing Technology*, *209*(1), 102–109. https://doi.org/10.1016/j.jmatprotec.2008.01.050
48. Uçar, M. K., Ucar, Z., Köksal, F., & Daldal, N. (2021). Estimation of body fat percentage using hybrid machine learning algorithms. *Measurement*, *167*, 108173. https://doi.org/10.1016/j.measurement.2020.108173
49. Li, D., Liu, J., & Liu, J. (2021). NNI-SMOTE-XGBoost: A novel small sample analysis method for properties prediction of polymer materials. *Macromolecular Theory and Simulations*, *30*(5), 2100010. https://doi.org/10.1002/mats.202100010
50. Dong, Q., Bai, S., Wang, Z., Zhao, X., Yang, S., & Ren, N. (2023). Virtual sample generation empowers machine learning-based effluent prediction in constructed wetlands. *Journal of Environmental Management*, *346*, 118961. https://doi.org/10.1016/j.jenvman.2023.118961

Publisher's Note Springer Nature remains neutral with regard to jurisdictional claims in published maps and institutional affiliations.

Springer Nature or its licensor (e.g. a society or other partner) holds exclusive rights to this article under a publishing agreement with the author(s) or other rightsholder(s); author self-archiving of the accepted manuscript version of this article is solely governed by the terms of such publishing agreement and applicable law.



Aslan Akdulum completed his PhD in Manufacturing Engineering at Gazi University. He is currently working as a researcher and lecturer in the Department of Machinery and Metal Technologies at Hacettepe University. He is working on modeling different machining methods with artificial intelligence-supported methods.



Yunus Kayir completed his PhD in the Department of Mechanical Education at Gazi University, Institute of Science, in 2001. He received the title of Prof. Dr. in 2024. He currently works at the Department of Manufacturing Engineering at Gazi University. He conducts his studies in the fields of computer vision, artificial intelligence, manufacturing systems modeling and analysis, multi-criteria decision-making, machining, and manufacturing.